Mineral Exploration with Natural Electromagnetic Fields

Morrison, H.F.[1], and Nichols, E.A.[2]

1. Engineering Geoscience, University of California at Berkeley and Ernest Orlando Lawrence Berkeley National Laboratory
2. Electromagnetic Instruments Inc., Richmond, California

ABSTRACT

Improvements in sensors, instrumentation, survey methodology, data processing and interpretation have rejuvenated methods of mineral prospecting using natural fields. The magnetotelluric method can now acquire excellent quality data across the entire natural field spectrum of interest, from 10^{-3} Hz to 10^{3} Hz. Continuous profiling of the surface impedance, or profiling of electric field alone referenced to a fixed magnetic measurement site, using arrays of in-line and orthogonal dipoles have proven very effective for mapping conductivity and detecting conductivity anomalies even in the presence of strong overburden inhomogeneities. Determination of the full impedance tensor permits the detection of both thin resistive and conductive vertical structures, provides a measure of the dimensionality of the subsurface and determines the deep or regional strike. MT profiling is particularly effective for mapping at depths of one to two hundred metres or more beneath conductive cover. An important practical advantage is that the results of these surveys can be presented in geologically interpretable form as resistivity vs. depth sections.

INTRODUCTION

There has been a significant increase in the past few years in the use of natural electromagnetic fields for mineral exploration. Developments in instrumentation, field procedures and data interpretation have encouraged a new look at natural field methods for both conductivity mapping and the detection of conductive targets. The best known survey technology is magnetotellurics (MT) [e.g., Vozoff (1991)], a method in which the conductivity structure of the ground is characterized by the ratio of orthogonal horizontal electric and magnetic fields at the earth's surface. This ratio of fields is known as the impedance and it could be used with any electromagnetic system but it is particularly appropriate with natural fields because one has no information about the actual source of the fields. Historically MT has been used principally for structural and tectonic studies of the deep crust using frequencies below 0.1 or 1.0 Hz. A related method of deep studies, usually referred to as geomagnetic depth sounding (GDS) (e.g., Schmucker (1970) or Gough and Ingram (1983) relies on simultaneous measurements at many sites of low frequency magnetic fields from induction currents in the earth. A parallel method using frequencies in the 100–500 Hz band enjoyed fleeting success in the 1960s (Ward et al., 1966; Sutherland 1970). This audio frequency magnetic (AFMAG) method relied on measurements of ellipticity and tilt angle of the magnetic field caused by induced currents. Sharing the same physics, the GDS and AFMAG methods differ only in frequency range and nomenclature. Another technique sharing the same principles using controlled source fields in the 15 to 25 kHz band is the VLF method (McNeill & Labson 1991).

For many years MT and GDS were used only at frequencies below 0.1 Hz simply because the natural em spectrum is weak between 0.1 and 3.0 Hz and the sensors were inadequate. The development of a new generation of low noise sensors and signal processing with the aid of remote reference (Gamble, Goubau and Clarke 1979) ushered in a new era for MT, the primary impetus for which was petroleum exploration (e.g., Warren et al., 1992; Morrison et al., 1996; Hoversten and Morrison, 1996). MT systems began acquiring data up to 500 Hz and it became apparent that MT might be useful for exploration for deeply buried mineral deposits, especially in conductive terrains. It also became apparent that the impedance measurement itself has some potential advantages over other em measurements especially when used in a continuous profiling mode.

With controlled sources the measured fields can be normalized by the source moment, and the known source-receiver geometry, and measurement of either *E* or *H* separately suffice to characterize the conductivity distribution in the ground. Only one hybrid scheme (CSAMT,

In "Proceedings of Exploration 97: Fourth Decennial International Conference on Mineral Exploration" *edited by* A.G. Gubins, 1997, p. 527–538

Zonge and Hughes, 1991) has evolved over the years which employs measurements of impedance from either a grounded electric bipole or loop source. In general, controlled source em (CSEM) methods use magnetic field sources and receivers because of the ease with which data can be taken with non-contacting systems. When only one field is measured there are strong reasons for measuring in the time domain since the secondary fields are measured in the absence of the much stronger primary or inducing field and this has long been considered a major advantage for CSEM time domain systems. In frequency domain impedance measurements we shall see that the electric fields can be thought of as the secondary fields and so electric fields normalized by the magnetic fields can approach the sensitivity of time domain measurements, The impedance approach basically eliminates the need for any coupling between source and receiver, eliminates any measurement of the source function (moment), and since the measurements are made in the frequency domain, the requirements for linearity and dynamic range of the field receiver are greatly reduced. From a theoretical point of view the electric field offers the highest resolution of subsurface structure. This is easily seen from the model of a vertical contact between two quarter spaces of different conductivity. Current normal to the contact is continuous and so the measured electric field on the surface is discontinuous in the ratio of the conductivity contrasts. Any magnetic component varies smoothly across the same feature. As we shall see later this inherently higher resolution of E compared to H persists as the contact is buried. Ironically, it is this extreme sensitivity to near surface inhomogeneities that has weighed against impedance methods because it has not been clear how to design configurations and filters to remove unwanted near surface effects while preserving the high resolution of deeper targets.

The measurement of the electric field and the perceived drawbacks of the sensitivity to near surface features have probably been the major reasons that impedance methods are not more widely used. It is certainly easier to survey large areas with inductive systems, even from the air, and avoid the practical difficulties of contacting the ground with measuring electrodes. However as depths of exploration have increased, and with many prospective areas buried under conductive overburden, targets are becoming beyond the reach of airborne methods and, increasingly, are testing the practical cost effectiveness of large loop or grounded dipole controlled source ground systems.

In this paper, we wish to revisit the role of natural field methods, especially magnetotellurics, for mineral exploration.

THEORY

The basic theory of the magnetotelluric method is reviewed by Vozoff (1991). The sources for fields in the 10^{-4} to 10^{3} Hz band are magnetohydrodynamic processes in the ionosphere/magnetosphere and lightning discharges in the earth ionosphere cavity. In either case the incident fields are well represented by incident plane waves and the impedance is a function only of the ground and not the source. Over a layered earth the reflection coefficient for magnetic fields is very close to one so the total field at the surface is twice the incident field. For the electric fields the reflection coefficient is close to minus one so the total electric field is reduced nearly to zero and E is the sensitive measure of conductivity. If the ground is inhomogeneous there will be gradients of electric field and secondary magnetic fields will be introduced, including a vertical component which would not be present over the layered half space (the reflection coefficient for H_z, for a plane wave TE mode, being close to minus one). The natural field spectrum increases rapidly below 0.1 Hz and has a broad gentle rise between 5.0 Hz and 500 Hz. Between 0.1 and 5.0 Hz, the fields are very weak and at times, and in some places, are at the noise levels of both the electric and magnetic field sensor systems. This part of the spectrum is often called the dead band. Further, em waves propagating in the earth-ionosphere waveguide from lightning discharges are severely attenuated in a band centered around 1000 Hz. Far from lightening activity, e.g., N. America in winter, there is virtually no energy in this band and natural field methods cannot be used.

The relationship between the induced fields E_x, E_y, and H_z and the inducing fields H_x, H_y is usually written as:

$$\begin{bmatrix} E_x \\ E_y \\ H_z \end{bmatrix} = \begin{bmatrix} Z_{xx} & Z_{xy} \\ Z_{yz} & Z_{yy} \\ T_{zx} & T_{zy} \end{bmatrix} \cdot \begin{bmatrix} H_x \\ H_y \end{bmatrix} \qquad [1]$$

where the T_{zx} and T_{zy} terms are the components of the Tipper.

The fields in this expression are measured fields and so strictly speaking the (H_x, H_y) vector is not the actual incident magnetic field but rather the sum of the incident field and a secondary field caused by the induced currents in the earth. A more general representation is that advanced by Egbert (1996) in which the column vector, x, of measured fields at a given site is the product of a two column transfer function matrix, U, for that site and a polarization vector representing orthogonal, true, incident fields, i.e.

$$|x| = |U||B| \qquad [2]$$

Of course we can never recover $|U|$ because $|B|$ is not directly measurable, but any relationship between the observed fields can be expressed with linear combinations of elements of the two columns of U.

This is also the starting point for Egbert's multivariate statistical approach to estimating the tensor impedances and transfer functions. Li and Pederson (1991) arrived at a similar description of the impedance in their elegant analysis showing that any source with multiple polarization yields an impedance relation that depends only on the frequency, geometry of the source receiver configuration and on the conductivity distribution, but not on the orientation or strength of the sources.

On the surface of an inhomogeneous ground we can expect strong variations in E and lesser variation in H. In traditional MT the impedances, and vertical fields expressed via the tipper, are measured at separate sites and variations of individual components over the surface are never measured. This procedure can cause severe interpretational problems because of the strong electric field dependence on shallow inhomogeneities. This distortion by near surface features is well illustrated by a small near surface block used in the analysis of Wannamaker et al. (1984) or Torres-Verdin and Bostick (1992), shown schematically in Figure 1. When the frequency is such that the skin depth within the block is much larger than the dimension of the block there is no induction in the block and the current flow is a simple dc perturbation of the current induced in the surrounding medium. The phase of the measured electric field is dictated by the induction response of the much larger surrounding medium. These low frequency responses are frequency independent and their effect persists throughout a sounding. The soundings for such a model are shown schematically in Figure 1. This static shift has been a major problem in MT and many solutions have been advanced for reducing or removing it. These have included shifting

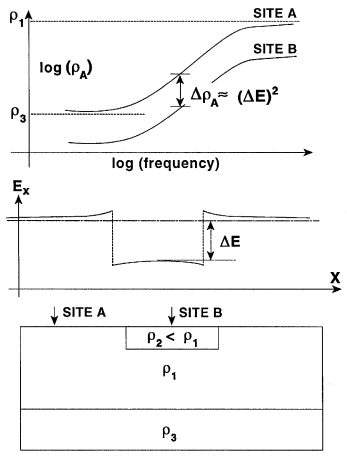

Figure 1: *Schematic illustration of the distortion of the electric field and shift of the sounding curves in the vicinity of a surficial conductor.*

local sounding curves into agreement if a deep regional feature is believed to lie beneath all the sites (Jones, 1988), correcting or shifting a sounding curve to be in agreement with an independent measure of background conductivity using another em technique (Sternberg et al., 1988), or introducing static shift as another unknown in a multisite inversion to a common 2-D model (as in the RR1 inversion of Smith and Booker (1991).

Torres-Verdin and Bostick (1992) and have presented a clear analysis of MT by linearizing the response of an arbitrary earth using the Born approximation in the integral equation formulation of the problem. Though restricted in practice to models with low conductivity contrasts, the physics of the response, including the phenomenon of static shift is clearly revealed. The approach showed the importance of correct spatial sampling of fields, it led to a simple spatial filter for reducing static shifts and it also led to a simple, fast, direct imaging scheme. We present a brief review of their analysis to provide a context for some of the interpretation schemes to be discussed below. This approach is described here in two dimensions for algebraic simplicity and illustration of the concepts. The analysis by Torres-Verdin and Bostick is in three dimensions. Chave and Smith (1994) have presented a similar analysis based on an extended version of the Born approximation with the objective of analyzing magnetic and electric galvanic distortion in tensor impedances.

For a two dimensional medium, the conductivity is a function only of x and z and we choose to describe it as a perturbation from a background conductivity, α_0, using the object function $O(x,z)$ defined by

$$O(x,z) = \frac{\sigma(x,z) - \sigma_0}{\sigma_0} = \frac{\Delta\sigma}{\sigma_0} \qquad [3]$$

In the presence of an inducing or primary field, secondary electric or magnetic fields are created by induced anomalous currents in the medium. At any point, the total field E_T is then the sum of the incident field E_0 and the scattered or secondary field E_S, i.e.,

$$E_T = E_0 + E_S \qquad [4]$$

with a similar representation for magnetic fields.

In the integral equation form for the solution the secondary field is expressed by an integral of the product of the scattering current, $\Delta\sigma E_T$, and the appropriate Green's function over the volume of the anomalous conductivity,

$$E_S(r) = \int_{r'} \Delta\sigma E_T(r') G_E(r,r') dr' \ldots \qquad [5]$$

where r is the coordinate (x,z) of the observed field, r' is the coordinate (x',z') of the scattering current, and G_E is the electric Green's function.

This is a non-linear equation and it can be solved numerically by methods outlined by Hohmann (1991) among others. A first order Born approximation to this equation can be made by assuming that the scattered field is small compared to the total field, which implies that $\Delta\sigma << \sigma_o$, and simply substituting the primary field $E_0(r')$ for $E_T(r')$ in Equation 5. Finally, if we assume the anomalous region is the entire lower half space, then

$$E_S(r) = \int_{-\infty}^{\infty}\int_{0}^{\infty} G_E(r,r')\Delta\sigma(r')E_0(r')dx'dz' \qquad [6]$$

In the MT problem for the TE mode the primary field in the half space of background conductivity α_0 is simply the y component:

$$E_{z0}(z') = E_{y0}e^{-ik_0 z'} \qquad [7]$$

where

$$k_0^2 = -i\sigma_0\omega\mu_0 \qquad [8]$$

With a little rearranging and the substitution of the object function in place of $\Delta\sigma$ we have

$$\frac{E_{yS}(x_r)}{E_{y0}} = -k_0^2\iint O(x',z')G_E(x'-x_r,z')e^{-ik_0 z'}dx'dz' \qquad [9]$$

If we Fourier transform both sides of this equation in x_r, i.e., along the line of observed data

$$\frac{E_{yS}}{E_{y0}}(k_{xr}) = -k_0^2\iint O(x',z')e^{-ik_0 z'}G(k_{xr},z')e^{ik_{xr}x'}dx'dz' \qquad [10]$$

Now the Green's function in horizontal wavenumber, k_x, domain is

$$G(k_{xr},z) = \frac{1}{|k_{xr}| + \sqrt{k_{xr}^2 - k_0^2}}e^{-i\sqrt{k_{xr}^2 - k_0^2}\cdot z} \qquad [11]$$

but $k_{xr}^2 + k_{zr}^2 = k_0^2$ and so in horizontal and vertical wave numbers

$$G(k_{xr}, z) = \frac{1}{|k_{xr}| + ik_{zr}}e^{-ik_{zr}z} \qquad [12]$$

If for convenience we set $S_z = i(k_0 + k_{xz})$, and with some rearranging, we get the following form for the spatial transform of normalized secondary field:

$$\frac{E_{yS}(k_{xr})}{E_{y0}} = \frac{-k_0^2}{|k_{xr}| + ik_{zr}}\iint O(x,z)e^{-S_z}e^{ik_{xr}x}dxdz \qquad [13]$$

For the TM mode the Greens function is composed of two parts and the final expression for the normalized scattered field is

$$\frac{E_{xS}(k_{xr})}{E_{x0}} = \frac{-k_0^2 + k_{xr}^2}{ik_{zr}} \iint O(x, z) e^{-S_z} e^{ik_{xr}x} dx dz \qquad [14]$$

We find that the transform of the observed field is simply equal to a Fourier and Laplace transform of the object function weighted by a filter or transfer function that depends on the frequency and the horizontal wave number. These two weighting functions, $-k_0^2/(|k_{xr}| + ik_{zr})$ for the TE mode and $(-k_0^2 + k_{xr}^2)/(ik_{zr})$ for the TM mode reveal some fundamental differences in the TE and TM mode responses for an arbitrary conductivity distribution. For the TE mode and the first term of the TM mode the amplitude of the ratio is in the form of a low pass filter. High horizontal wave numbers are attenuated. This means that high frequency wave numbers in the object function are smoothed in the observed TE and part of the TM response. Further the response assymptotes to a constant at very low wavenumbers because these are the induction components of the two modes. The second term in the TM is quite different: it produces a high pass response. This is the dc response of the TM mode which Torres-Verdin called the static response. High wavenumber components in the object function are faithfully carried over to high wavenumber components in the response and this explains the sensitivity of the electric field to near surface inhomogeneities.

The second important conclusion from this analysis is that the information about the conductivity distribution is completely contained in the normalized electric field data. Either of the above equations for the scattered electric field can be inverse transformed to yield the object function. For example, for the TE mode we can write

$$O(x, z) = \frac{1}{i(2\pi)^2} \iint \left(\frac{|k_{xr}| + ik_{zr}}{-k_0^2} \cdot \frac{E_{yS}(k_{xr})}{E_{0y}} \right) e^{S_z} e^{ik_{xr}x} dk_x dS \qquad [15]$$

This is a direct solution for the conductivity distribution. It is an inverse Laplace and Fourier transform of the weighted spatial transform of the observed normalized secondary field. Expressed in this fashion it is clear that to resolve the conductivity the electric field has to be sampled continuously on the surface, or at least the sampling must satisfy a standard Nyquist criteria based on the wave number content of the conductivity distribution at the surface. If the surface is inhomogeneous and the electric fields are sampled at sites too widely spaced the electric fields are aliased, the spatial transform is in error and the conductivity distribution cannot be recovered. It also shows that the conductivity can be obtained from electric fields provided an estimate can be made of the value of the incident electric field on a half space of the background conductivity, σ_0. On such a half space $E_0/H_0 = Z_0$ and if at least one point on the profile lies over a section that is even approximately 1-D then H_0 is known (it is half the observed horizontal field) and a background σ_0 can be taken from the 1-D interpretation. This is the basic theoretical explanation for using electric field profiling, referenced to a fixed magnetic site, rather than profiling impedances using magnetic fields at each electric field measurement point. This results in considerable logistic simplification since magnetic field sensors must be buried in the ground to reduce wind noise and ground vibration noise and this can often be a difficult and rate limiting task.

This formulation of the problem also shows that if the data are sampled correctly, they can be spatially filtered in such a way as to remove the non-inductive or static response from the TM data. It was this property that led Bostick (1986) to design an adaptive spatial filter which would reduce the static responses without overly smoothing the inductive responses from deeper in the section. This is the underlying principle of the EMAP process.

Finally, although an inverse Laplace transform is unstable, with suitable regularization Torres-Verdin derived a robust inversion algorithm that has proven to be very useful for fast approximate imaging (Torres-Verdin 1991; Torres-Verdin and Morrison 1991; Marigiano 1994). In practice it has turned out to be better to use a Rytov approximation and we will show the results of this inversion in the sections that follow.

In the full 3-D analysis using this approach Torres-Verdin and Bostick (1992) also show how orthogonal inducing fields can be coupled by 3-D features. This implies that phase distortion can arise when currents whose phase has been set by induction in one direction are statically distorted into another direction. Furthermore they also show that for 3-D bodies there can be frequency dependent distortions of the magnetic field by inhomogeneities even at frequencies below which there is no induction in the body. Although they show that this effect is small for reasonable contrasts and low frequencies, it is a potential problem for impedance measurements. It is not a problem for electric mapping provided the reference magnetic site is not in the vicinity of such a distorting body.

The importance of correct sampling and the possibility of direct imaging algorithms led us to concentrate on continuous electric field profiling. In a sense we have revisited the telluric profiling that was used in the sixties (see, for example, Yungul 1966). In this technique the electric fields of contiguous dipoles on a profile as a function of frequency were interpreted in terms of relative conductivity variations beneath the profile. Including the magnetic field converts this process to continuous impedance profiling and permits inversion to absolute conductivity.

The model study below which illustrates some of these concepts also shows the results of several current inversion procedures. Static effects severely distort inversion results basically because of the aliasing effects described above and so inversions also benefit greatly from continuous coverage. In this paper we have confined our analysis to the use of two dimensional models. This assumption of two dimensionality is certainly a weakness in the interpretation of MT data as it is in many other em and electrical methods. In many geologic situations, a near surface and regional strike can be deduced from the geologic map, other geophysical data, or from the results of a few carefully selected MT sites. Once a near surface strike direction has been determined the MT profile should be conducted perpendicular to it. Fortunately, the impedance tensor itself carries a measure of site dimensionality. For a 2-D geology, the ratio of $(Z_{xx} + Z_{yy})/(Z_{xy} - Z_{yx})$, called the *Skew*, is zero and it departs from zero as three dimensional effects become important. Numerical modeling over reasonable 3-D features show skew values reaching 0.3 to 0.5. Regional strike can often be determined even in the presence of local 3-D static distortion using the tensor decomposition methods of Groom and Bailey (1989), and such an analysis should be carried out at regular intervals along a profile to ensure that the assumed strike directions are not changing. The Groom-Bailey decomposition is also useful in determining whether there is significant static distortion (aliasing) in the cross line, strike, components.

We present a brief review of the properties of natural field responses and of some of the two dimensional inversion schemes using the three models shown in Figures 2a, 4a, and 5a.

MODEL STUDY

This is not intended as a comprehensive model study but rather a synopsis of model simulations which illustrate some fundamental characteristics that will be seen in the field results presented later. The first, Figure 2a, is illustrative of a common prospecting target, similar in many respects to the Eloise one body in northwest Queensland, Australia, described by Brescionini et al. (1992). The target is a thin vertical dike of conductance, 1000S (the conductivity thickness product, σt) in a resistive host and under a one ohm-metre overburden one hundred metres thick. The model of Figure 4a is illustrative of vertical or subvertical silicified zones, which are usually more resistive than their surroundings, and are currently targets for gold exploration in many parts of the world. Figure 5a is representative of the general problem of mapping conductivity structures beneath a highly inhomogeneous overburden.

For each of these models we have calculated the apparent resistivity, ρ_a, and impedance phase for both the TE (*E* parallel to strike) and TM (*E* perpendicular to strike) mode and plotted the results as contours in frequency-horizontal distance coordinates. We have also plotted the magnitude of the tipper for the TE mode. The tipper is presented in conventional MT surveys, but tilt angle and ellipticity have been the parameters of choice in AFMAG and VLF surveys.

The TM response for the vertical conductor is below the detection threshold for any MT system and is not shown. In a circuit analog it can be said that a small resistor in series with large ones has no effect on the total resistance. This target would be missed with any em technique in which the incident or primary electric field was perpendicular to the strike. The TE response, Figure 2b and 2c, is much different and reveals a pronounced and easily detectable broad apparent resistivity low over the target. The maximum anomaly is at about 1.0Hz and a profile of ρ_a at 1.0 Hz shows a drop from 6 ohm-m to less than one ohm-m over the target. The tipper response at 1.0 Hz, Figure 2d, is also substantial and well above the noise level for tipper measurements in MT as are the ellipticity and tilt angles (not shown).

This model illustrates two very important points for survey design. There is no response for TM so an in-line *E* dipole profile perpendicular to strike will miss the target. The response for TE is excellent but would require dipoles in the strike direction to be detected. Because the anomal is broad, the sampling need only be on the order of 200 metres to detect it. However care must be exercised to deploy the profile perpendicular to near surface strike to minimize aliasing of the TE mode. Note that if the profile is oriented at an angle to the deeper strike of the target, the impedances can be rotated to coincidence with the deep feature provided the TE mode measurements are not aliased.

To put this response into some perspective with respect to other em methods we have calculated the transient response for receiver profiles perpendicular to a vertical magnetic dipole 200 m to the right of the target as shown in Figure 7. Contours of secondary vertical field amplitude vs. horizontal position and time showed that the maximum secondary field response from the target occurs 50 m to the left of the target and at 20 m seconds. The transient decay curves in Figure 3 shows the total field T, the field of the layered half space alone, L, and the secondary field, S. The distortion of the layered field by the target is only 50%, compared to a factor of 6 for the tipper.

This comparison of methods is not rigorous. The MT response would be reduced once the strike length became less than four or five times the depth, and the TDEM response is for a sheet (of the correct conductance) that is 400 m in strike length and for a dipole rather than a large loop source. Nevertheless the strong TE response at 1 Hz for a method requiring no large source shows the potential for the method. Further the strong tipper anomaly shows that this target would be easily detected with a modern 8Hz AFMAG system.

The response of a vertical resistive target beneath overburden, Figure 4a, shows the complementary character of the TE and TM modes when the contrast of the target is reversed. Now the TE response is negligible but the TM currents are blocked by the vertical resistive barrier, current is shunted up into the overburden measuring the measured electric field in the profile direction and causing a broad distinctive anomaly in the apparent resistivity. There is only a small phase anomaly at high frequencies when there is inductive interaction near the top of the dike.

The TM apparent resistivity section for the model with the surface inhomogeneities, Figure 5b, shows the dramatic striping that is characteristic of static shifts in this mode. The electric fields are shifted up or down by a frequency independent factor once the frequency falls below a point where the induction number of the inhomogeneity becomes negligible, and so the distorting effect on the apparent resistivities persists through the section to arbitrarily low frequencies. The phase section, Figure 5c, shows the complimentary effect that there is no phase distortion once the induction response becomes negligible below about 10 Hz. The phase responses of the two bodies are mixed with the overburden phase response and in this case phase is not a good indication of the targets. The low pass response of the TE mode is evident in the apparent resistivity section of Figure 5d as is the fact that the TE amplitude response diminishes at low frequency. The induction effects at high frequency in the near surface bodies cause more phase mixing of overburden and body responses than in the TM mode making it even harder to distinguish the bodies in this mode, Figure 5e. The much smoother response of the TE model shows graphically why the TM response has inherently higher spatial resolution in the direction perpendicular to strike. Unfortunately, the static shifts mask this advantage for deeper bodies.

We have used the model of Figure 5a to illustrate two of the inversion schemes that we have used with field data. Again, this is not intended to be a rigorous comparison of inversion techniques, but to give the reader some inkling of the effectiveness of inversion methods on known models.

The first process we describe is the direct Rytov imaging scheme introduced above in the discussion on theory. There we showed that the object function, the distribution of conductivity perturbations about a background half space conductivity, can actually be written in terms of inverse Fourier and Laplace transforms of the profile electric field data. The inverse Laplace transform is unstable and to carry out the process it must be regularized. Nevertheless Torres-Verdin (1991) derived a practical algorithm which produces conductivity distributions directly from the field data. We refer to this as the Born or Rytov direct imaging scheme. The method is sensitive to truncation effects with short profiles and to the choice of background resistivity and like the EMAP approach it does not yield a direct measure misfit. This inversion is shown in Figure 5f.

Finally, we have used the well known 2-D Rapid Relaxation Inverse (RRI) of Smith and Booker (1991), and these results are shown in Figure 5g.

The Rytov image takes only minutes on a workstation and at least for this model yields a useful inversion. The RRI can take up to an hour on the same machine and has the distinct advantage of yielding quantitative measures of the goodness of fit. The various input parameters, ρ_A are phase for the TE and TM modes can also be weighted by assigned or

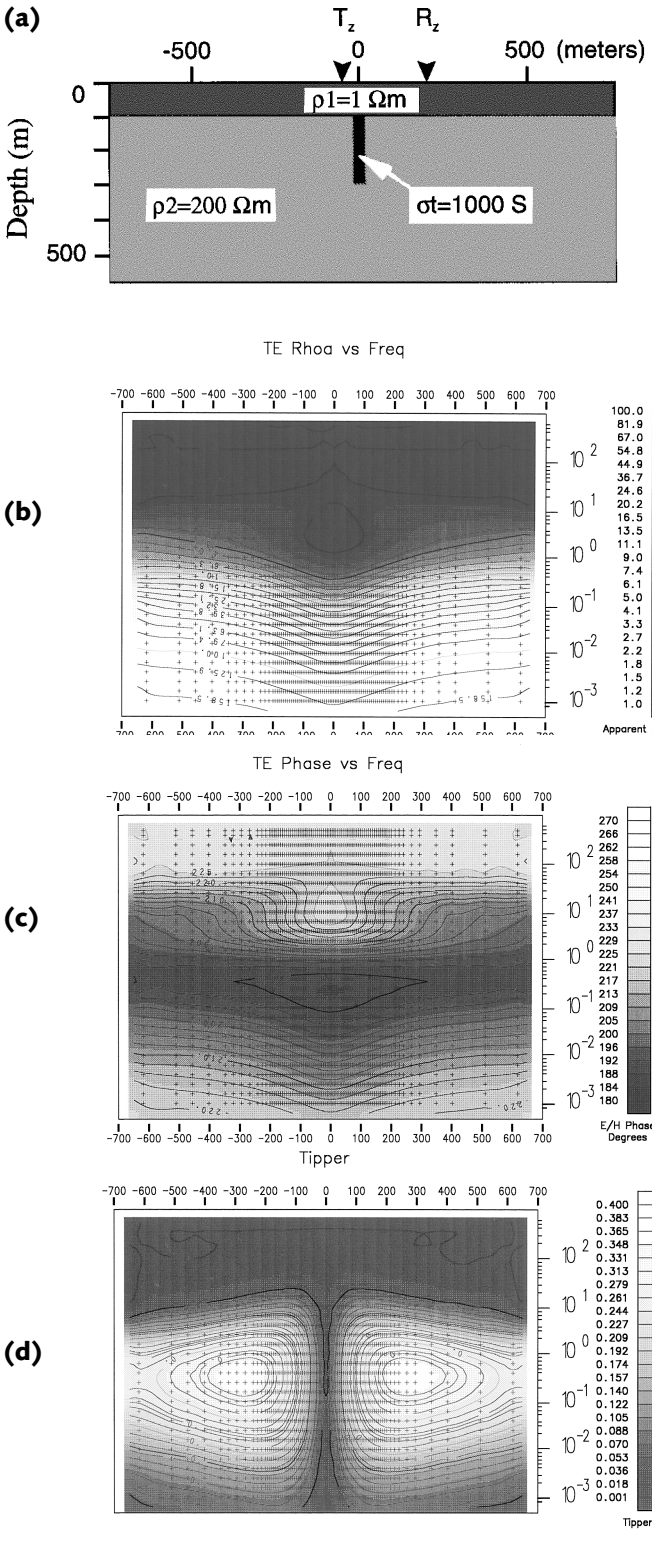

Figure 2:
*(**a**) Model of a conductive dike beneath a conductive overburden (**b**) ρ_A for the TE mode (**c**) phase for the TE mode (**d**) Tipper. Horizontal scale in metres, vertical in frequency for (**b**), (**c**), and (**d**).*

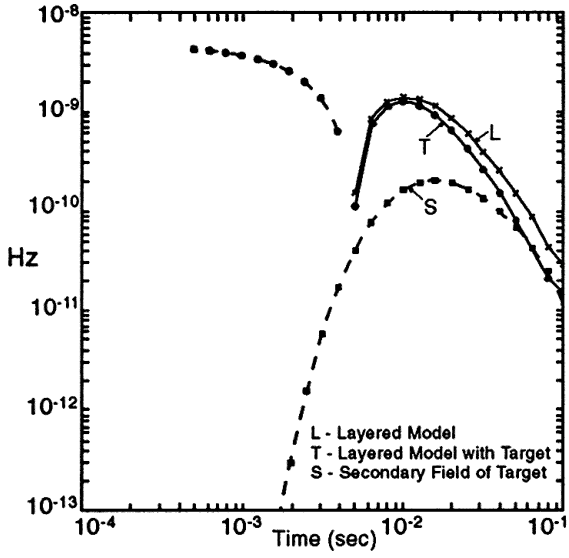

Figure 3: *Transient response for the total vertical field, T, the vertical field with no target, L, and the secondary vertical field, S, alone. The fields are for a receiver at location R and a vertical dipole source at location T_z in Figure 2a.*

measured errors so that modes known to be sensitive to certain features can be emphasized in the inversion. As a general rule we perform fast approximate inversions in the field which become first guess models to more rigorous inversions carried out later.

FIELD EXAMPLES

Australia

The first field results are from a profile taken over a massive sulfide deposit in the Eastern Fold Belt of the Mt. Isa Inlier in northwest Queensland. The mineralization is similar to the Eloise Cu-Au deposit described by Brescianini et al. 1992. Eloise is a generally vertical, thin, conductive (1000S) massive sulfide with considerable strike extent lying within Early to Middle Proteozoic rocks of the Eastern Fold Belt. The Proteozoic rocks are covered at the Eloise deposit by up to 50 to 70 m of flat lying sediments with resistivities in the 2–4 ohm-m range. Broadly speaking this class of deposit can be modeled by the thin vertical conductor shown by the model in Figure 2a.

The MT profile was laid out perpendicular to strike and used the full orthogonal configuration with 100m dipoles, and a frequency band of 10^{-2} to 200 Hz. The data quality was excellent with the exception of a period of very low signal level in the dead band, 0.1 to 1.0 Hz, during acquisition at the eastern end of the line (800–1200 m). The profile was 1.2 km long.

The apparent resistivity and phase sections for the TM mode are shown in Figure 6a, 6b. The section appears one dimensional with a surface resistivity on the order of 2 to 5 ohm-metres increasing to several hundred ohm-metres at depth. The phase data also reflects a 1-D section with no lateral induction variations. The TE and TM data are roughly the same above 10.0 Hz; both show a decreasing resistivity of the surface layer to the right of the figure. The TE also sees a surface segment

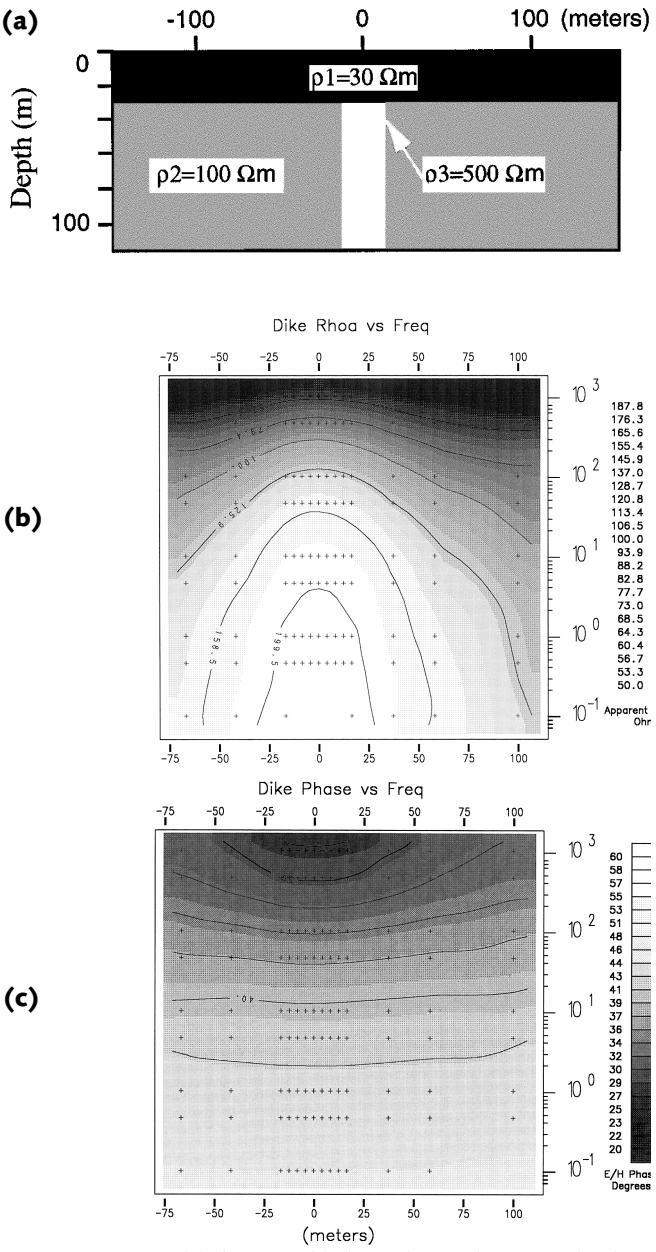

Figure 4: *(**a**) Model of resistive dike beneath a conductive overburden: (**b**) ρ_a for the TM mode: (**c**) phase for the TM mode. Horizontal scale in metres, vertical in frequency for (**b**) and (**c**).*

between 500 m and 800 m appears more conductive and which has a small associated phase anomaly. Since this is not seen in the TM mode, it must be associated with a surface feature off profile and along strike. The two single station phase anomalies are the result of the noise mentioned above. The apparent resistivity and phase results for the TE mode below 10 Hz, Figure 6c, 6d show the characteristic response of the TE mode for a thin vertical conductor. The apparent resistivities plunge to less than 10 ohm-metres in a relatively narrow zone beneath 600 m.

The major feature of this profile is the strong TE anomaly which develops for frequencies below 10 Hz. Skin depth considerations alone suggest that this conductor must be at least 100 m deep. The RRI inversion of both the TE and TM modes for this profile is shown in Figure 6e. The inversion shows a conductive surface layer and a broad conductive zone with a peak coming up to within about 100 m of the surface beneath 500 m. Drilling has confirmed the existence of mineralization at this site but depths and extent and the results of other geophysical surveys have not been published. As intimated in the study by Brescianini et al. (1992), the CSEM method was close to its depth of exploration limit at Eloise. As the model of Figure 2 and the data from this survey show, the anomaly is clear and distinct in the MT data below 10 Hz even with a depth of 100 m.

Carlin District, Nevada

The second field example is a profile conducted in the Carlin "trend" near the town of Carlin, Nevada. The northern Great Basin of Nevada contains classic examples of regional mesothermal disseminated gold deposits associated with coeval magnetism and intense hydrothermal activity (Seadorf, 1991). The region is currently the world's third largest gold-producing region.

Typically, the gold occurs in fine-grained disseminated deposits in discordant breccias and stratabound concordant zones. Although carbonates appear to be the most favored host lithology to the mineralization, the deposits are hosted by a wide range of lithologies and also occur in a wide variety of fractures and fault zones that are oblique to stratigraphic contacts. This implies that the mineralization is opportunistic and exploits structural weaknesses, rather than being stratigraphically controlled (Seedorf, 1991).

Individual deposits are thought to be distal products of magmatic-hydrothermal systems and/or precipitated in a deep zone of mixing between normally pressured and overpressured fluids (Figure 2, Kuehn and Rose, 1992, 1995). They tend to be localized along structural features such as thrusts, high angle normal faults and upright folds. Several, but not all, of the deposits appear to be constrained to two broad NW-trending structurally-controlled linear belts 200–300 km in length known as the "Carlin" and "Cortez" trends. These trends, however, do not correspond to any obvious exposed structure and are inferred to represent deep basement structural controls. However, the geophysical expression of these inferred structures is enigmatic.

The MT profile was laid out perpendicular to the Carlin "trend." The dipole length was 100 m with contiguous dipoles in the line direction and 100 m orthogonal dipoles, in the strike direction, every 100 m. This configuration is referred to as full orthogonal. The profile line was 4.7 km long. The survey was conducted in winter which is a time of low signal level in the 3.0 to 500 Hz band. Nevertheless, a good set of data in the 0.3 to 200 Hz band was collected. A more complete description of this survey itself has been presented by Morrison et al. 1990.

In the vicinity of the traverse gently dipping Miocone valley fill sediments unconformally overlie thrust slices of Paleozoic miogeoclinal rocks of the Roberts Mountain thrust formed during the late Devonian-Mississippian Antler orogeny (Pzu, Pzl, Figure 7g). There has been intense mineral exploration activity in the area and geological mapping and drilling constrains the configuration of the Tertiary fill and the unconformity. The underlying Paleozoic sequences as shown in the SW–NE cross-section, Figure 7g, are dominated by clastic rocks to the west and carbonate rocks to the east implying that the thrust is buried beneath the unconformity surface. The mineralization (uneconomic) that was encountered between stations 15 and 30 (Figure 7g) is located between two mapped faults in Devonian limestone.

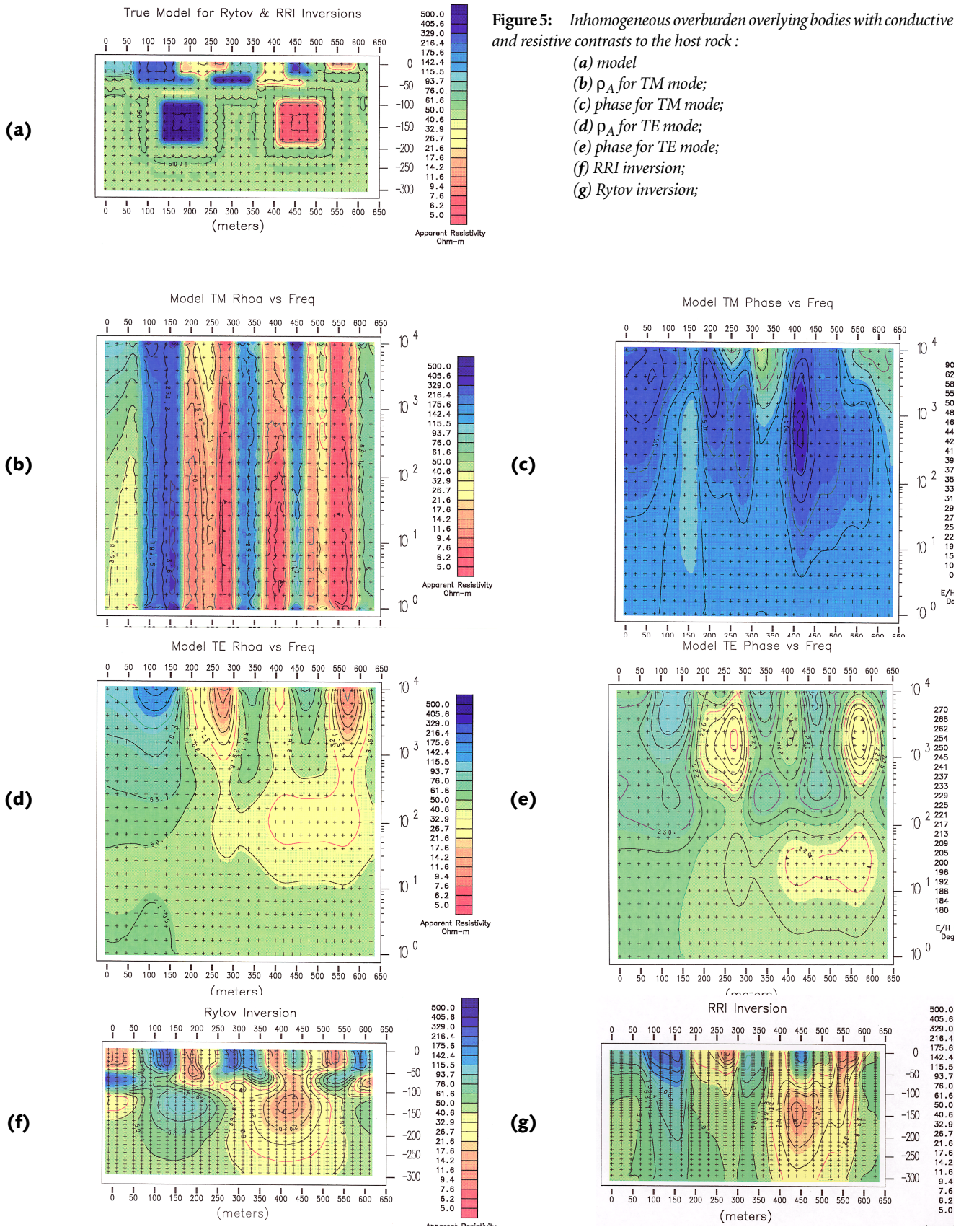

Figure 5: *Inhomogeneous overburden overlying bodies with conductive and resistive contrasts to the host rock :*

*(**a**) model*
*(**b**) ρ_A for TM mode;*
*(**c**) phase for TM mode;*
*(**d**) ρ_A for TE mode;*
*(**e**) phase for TE mode;*
*(**f**) RRI inversion;*
*(**g**) Rytov inversion;*

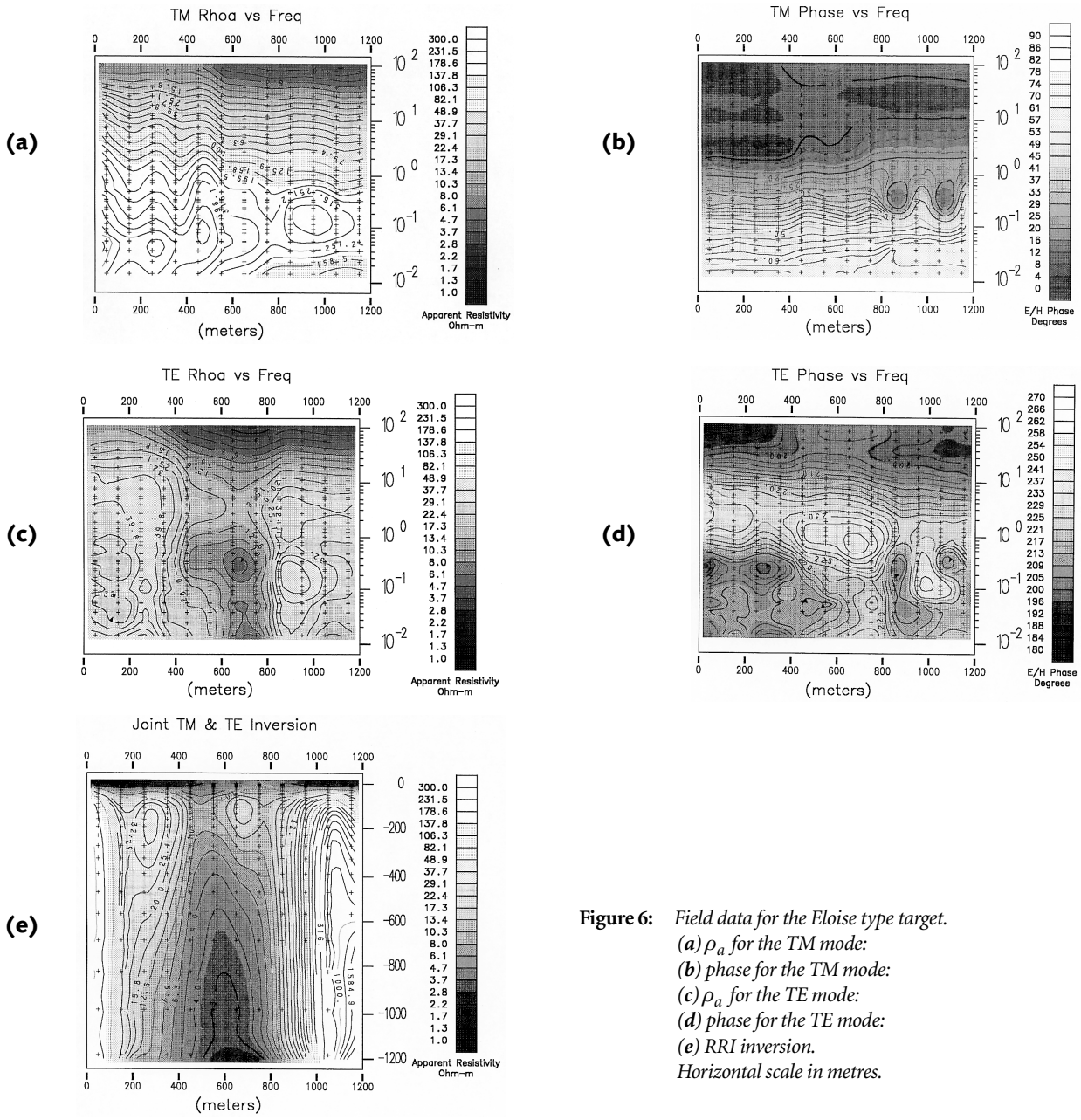

Figure 6: *Field data for the Eloise type target.*
*(**a**) ρ_a for the TM mode:*
*(**b**) phase for the TM mode:*
*(**c**) ρ_a for the TE mode:*
*(**d**) phase for the TE mode:*
*(**e**) RRI inversion.*
Horizontal scale in metres.

The apparent resistivity and phase sections for the TM and TE modes are presented in Figure 7a, 7b and 7c, 7d, respectively. The impedance strike direction was consistently perpendicular to the profile. The skew for the profile is shown in Figure 7f and it shows that the 2-D assumption is valid for all but the eastern end of the line at low frequencies. The high skews near the surface reflect high noise in the impedance estimates at the high frequencies.

The TM profile does not display serious static shift distortions and the data itself reveals the presence of an inhomogeneous generally conductive formation (the Tertiary) overlying more resistive units on the eastern portion of the line at depth. Lateral discontinuities reflect the fault contact between different basement units. There is no marked conductivity anomaly associated with the mineralization encountered in the drilling—a discouraging, but common, occurrence in prospecting for disseminated mineralization with EM.

The TE sections, Figures 7c, 7d, reveal a similar structure in the near surface, above 100 Hz, but there is a pronounced, narrow, resistivity low between 3500 and 4000 m. The resistivity anomaly is accompanied by a distinct phase anomaly, Figure 7d, which indicates the presence of a thin, vertical conductor in the Paleozoics. In this survey, when vertical fracture zones which may have been fluid conduits are prime targets, the TE coverage was critical in detecting this zone.

The data were interpreted with the RRI inversion code of Smith and Booker and the resulting resistivity depth section is presented in Figure 7e. Both modes were inverted simultaneously and the simulated data from the inversion model match both the TE and TM data very well. The only exception is at the eastern end of the profile at depth where the skew section has already shown that a 2-D model may not be appropriate.

The inverted section shows a narrow steep conductor beneath 3400 beginning roughly at the unconformity and extending to at least 2000 m.

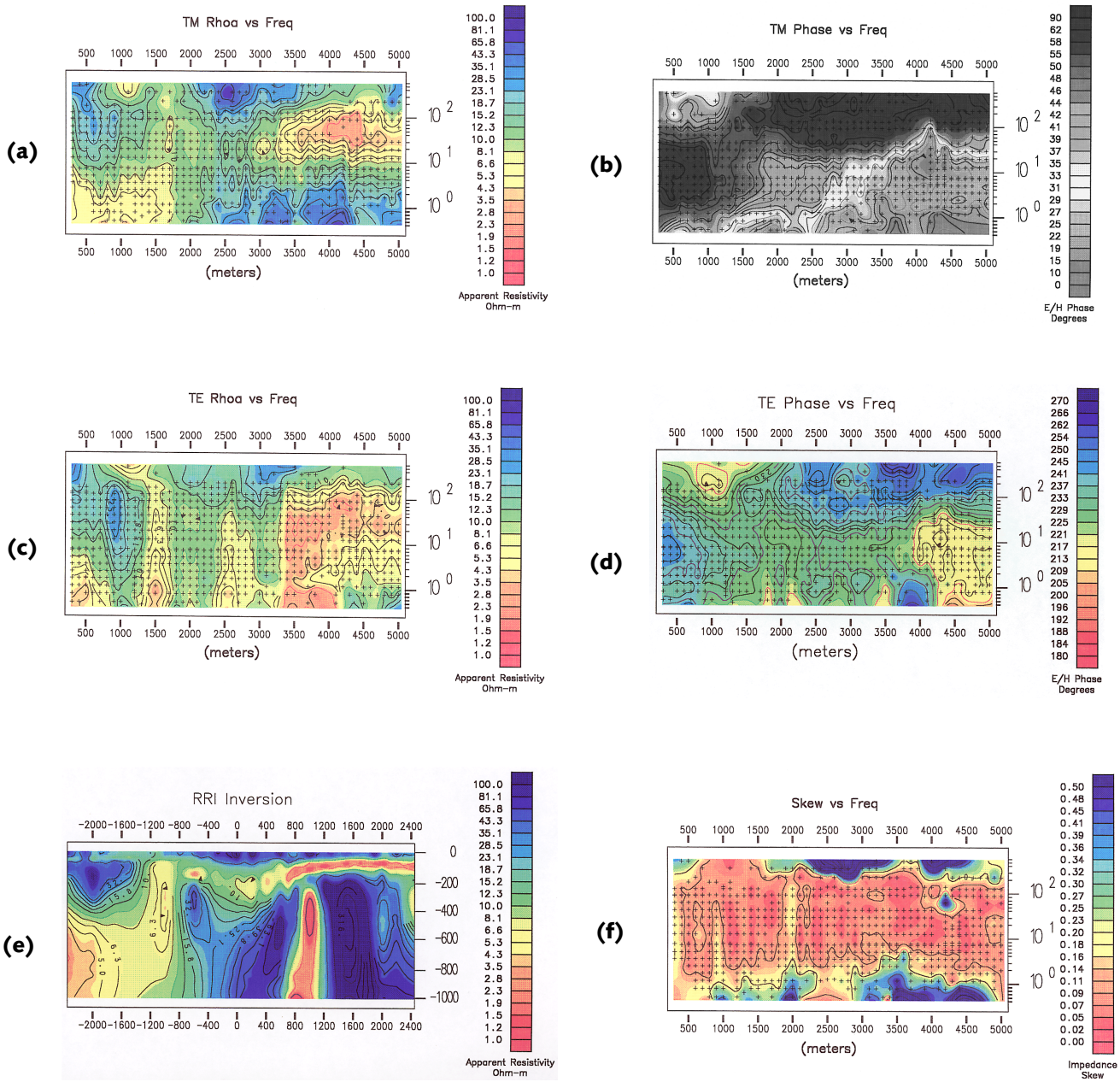

Figure 7: *Field data for the Carlin 1 profile:*
*(**a**) ρ_a for the TM mode;*
*(**b**) phase for the TM mode;*
*(**c**) ρ_a for the TE mode;*
*(**d**) phase for the TE mode;*
*(**e**) RRI inversion;*
*(**f**) skew;*
*(**g**) geological cross section.*
Horizontal distances in metres.

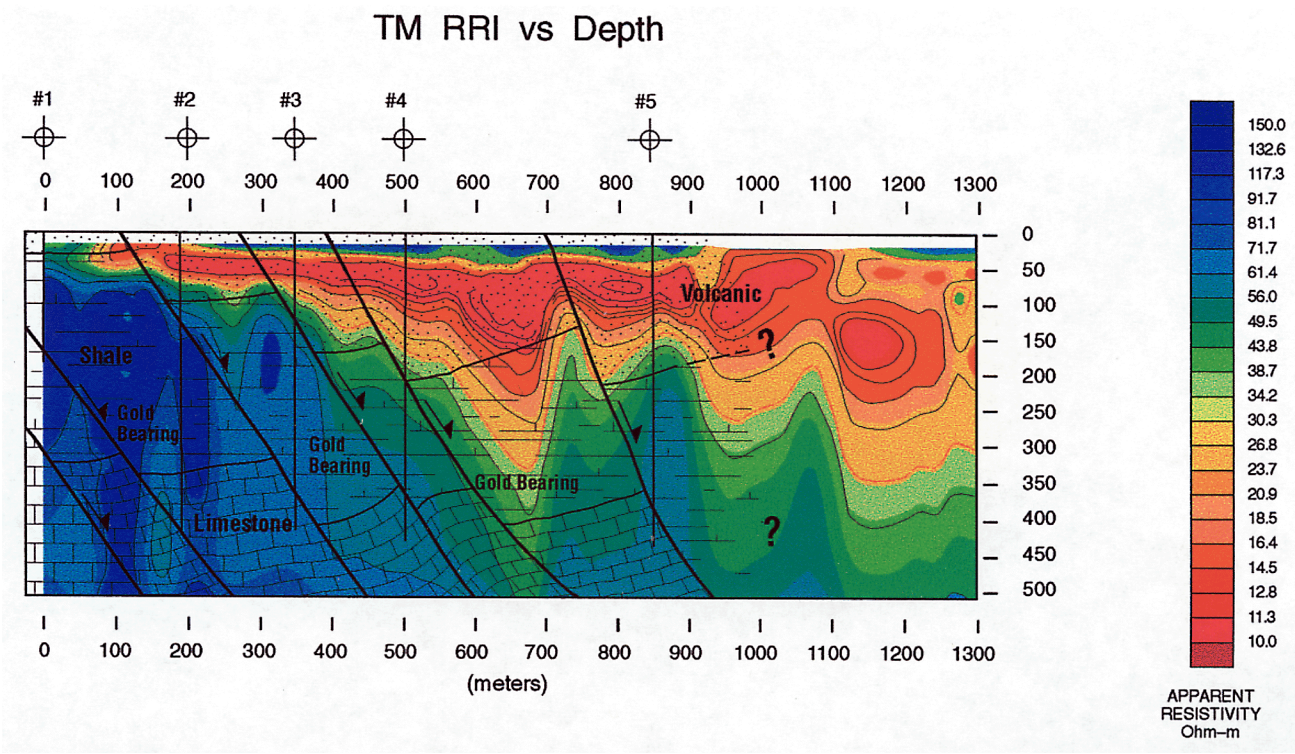

Figure 8: *RRI inversion of the Carlin II profile, with superposed drill hole geology.*

The feature is robust in the inversion—it is required to minimize the misfit. The strike is also well defined and it lies perpendicular to the profile and hence parallel to the Carlin trend. This feature was not detected in the CSAMT survey (scalar and TM mode) or in the dipole-dipole I.P. survey where it was probably too deep. It represents a potentially important target and its detection also shows that MT may be actively useful in mapping deep structural controls on mineralization. Apart from this detection of a deep conductor, we have shown that there is a strong correspondence between the MT image and the subsurface stratigraphy and structure along the section as obtained from the drill holes.

Carlin District II, Nevada

The last field example is taken from a survey in a different geological setting in the same Carlin District described in the first example. Here the geologic model consists of a roughly layered sequence of Paleozoic rocks overlain by volcanics. The basal sequence is limestone, which is overlain by shale, and then by the volcanics. Surface mapping shows successive normal faulting. Mineralization is suspected to be associated with the shales, possibly preferentially in the vicinity of the normal faults. In this study, the depths of interest were between 20 m and 500 m—considerably shallower than in the above two survey areas, and it was realized that frequencies up to 10 kHz would be needed. The survey was conducted using natural fields up to 700 Hz and a controlled source orthogonal vertical loop transmitter was used to obtain results in the 1 to 10kHz band. This system has been described by Nichols et al. (1994). The advantage of this hybrid survey is that the controlled source is only needed above 1000 Hz so that far field behavior can be achieved with a source-receiver separation of only a few hundred metres. At such small spacing the moment requirement is reduced and a portable transmitter with two orthogonal loops becomes feasible. Such a source provides two polarizations of the field which suffice for full tensor impedance measurements.

The strike direction was clearly evident in the geologic map and the profile was laid out perpendicular to strike. The dipole length was 50 m and the profile was 1.3 km long. The objective of the survey was to map the subsurface faults and statigraphy with the highest possible resolution in the profile direction. The apparent resistivities for the TM mode revealed a structure of increasing resistivity with depth and of increasing thickness of the low resistivity unit to the east (right). There were no significant static shifts evident although the apparent resistivity section showed considerable lateral variation. The TM phase section was remarkably uniform reflecting a wedge of surface conductor thickening to the east. The natural field and controlled source impedances overlapped very well around 1000 Hz and confirmed that the stations on the line were indeed in the far field of the source.

The data were inverted with the RRI code and the resistivity depth section is shown in Figure 8. This figure also shows the geological section derived from the five drill holes whose locations are shown on the figure. The resistivity cross section depicts the subsurface structure and lithology very well and in fact may reveal details that could not have been seen with the drill holes. It is apparent that the volcanics thicken by successive normal faulting with more unmapped faults around 850 m and 1050 metres being responsible for a thickness of several hundred metres to the right of the section. There appears to be no resistivity distinction between the limestone and shale.

CONCLUSIONS

We have seen that natural field methods, in this case magnetotellurics, provide a valuable means to map the conductivity and to detect conductors or resistors at depths where conventional em may not be logistically or cost competitive.

We have found that excellent data quality can now be achieved from 10^{-3} to 10^{3} Hz using a carefully installed remote reference station for an entire survey. Further we have shown that surveys can be conducted using electric measurements referenced to a fixed magnetic station on the line. For many structural studies in-line components of *E* provide the maximum resolution and dipoles in the strike direction are not needed. As a practical matter, it is important to monitor local and regional strike, and skew, along the line and we have found that deploying one orthogonal dipole in the strike direction for every 3 to 5 in-line dipoles usually suffices.

Perhaps a major advantage of the natural field, plane wave, methods is that inversion or imaging algorithms are available so that field data can rapidly be converted to resistivity sections. These sections are rich in detail and present the results of the survey in a manner which allows immediate geological interpretation.

ACKNOWLEDGEMENTS

We wish to thank BHP Minerals, Newmont Exploration and Placer Dome for permission to publish the geophysical and geological data in this study. The imaging research was supported in part by the Office of Basic Energy Sciences, Engineering and Geosciences Division, of the U.S. Department of Energy under contract no. DE-AC03-76SF00098. Data processing, modeling, and inversion studies were supported in part by a research consortium consisting of BHP Minerals, CRA Exploration, MIM Exploration, and Placer Dome Inc. Our thanks to Erika Gasperikova and Ted Asch who actually did the majority of the modeling and data processing for this project.

REFERENCES

Bostick, F.X., Jr., 1986, Electromagnetic array profiling (EMAP): 56th Am. Internat. Mtg., Soc. Expl.: Geophysics, Expanded Abstracts EM2.1, 60-61.

Brescianini, R.F., Asten, M.W., and McLean, N., 1992, Geophysical characteristics of the Eloise Cu-Au Deposit North West Queensland Exploration: Geophysics, 23, 33-42.

Chave, A.D., and Smith, J.T., 1994, On electric and magnetic galvanic distortion tensor decompositions: Journal, Geophysics Res., 99B3, 4669-4682.

Egbert, G.D., 1997, Robust multiple-station magnetotelluric data processing: Geophysics, Journal, Intnl. (in press).

Gamble, T.D., Goubau, W.M., and Clarke, J., 1979, Magnetotellurics with a remote reference: Geophysics, 44, 53-68.

Gough, D.I., and Ingham, M.R., 1983, Interpretation methods for magnetometer arrays: Reviews of Geophysics and Space Physics, 21, 805-827.

Groom, R.W., and Bailey, R.C., 1989, Decomposition of magnetotelluric impedance tensors in the presence of three-dimensional galvanic distortion: Journal, Geophysics Res., B, 93, 1913-1925.

Hohmann, A.W., 1988, Numerical modeling for electromagnetic methods of Geophysics; in Nabighian, M.N., Ed., Electromagnetic methods in applied Geophysics—theory, v1, Chap. 5, 314-364.

Hoversten, G.M., and Morrison, H.F., 1996, Papua New Guinea MT; Looking where seismic is blind: Geophysical Prospecting, 44, 935-961.

Jones, A.G., 1988, Static shift of magnetotelluric data and its removal in a sedimentary basin environment: Geophysics, 53, 967-978.

Kuehn, C.A., and Rose, A.W., 1995, Carlin gold deposits, Nevada: Origin in a deep zone of mixing between normally pressured and overpressured fluids: Economic Geology, v. 90, p. 17-36.

Li, X., and Pederson, L.B., 1991, Controlled source tensor magnetotellurics: Geophysics, 56, 1456-1461.

Maregiano, P., 1994, Imaging electromagnetic data in the wavenumber space: Report for degree of Master Science, Dept. of Materials Science and Mineral Engineering, University of California, Berkeley.

McNeill, J.D., and Labson, V.F., 1991, Geological mapping using VLF radio fields; in Nabighian, M.N., Ed., Electromagnetic methods in applied geophysics, v2, Application, Chap 7, S.E.G., Tulsa.

Morrison, H.F., Nichols, E.A., Torres-Verdin, C., Booker, J.R., and Constable, S.C., 1990, Comparison of magnetotelluric inversion techniques on a mineral prospect in Nevada; Exp. Abs, 60th Annual International Mtg., SEA, San Francisco, Sept. 23-27.

Morrison, H.F., Shoham, Y., Hoversten, A.M., and Torres-Verdin C., 1996, Electromagnetic mapping of electrical conductivity beneath the Columbia basalts: Geophysical Prospecting, 44, 963-986.

Nichols, E.A., Morrison, H.F., and Clarke, J., 1988, Signals and noise in magnetotellurics: Journal, Geophysics Res., 93B, 13743-13754.

Schmucker, V., 1970, Anomalies of geomagnetic variations in the southwestern United States: Bulletin, Scripps Inst. Oceanography.

Seedorf, E., 1991, Magmatism, extension and ore deposits of Eocene to Holocene age in the Great Basin-Mutual effects and preliminary proposed genetic relationships; in Raines, G.L., and Wilkinson, W.H., eds., Geology and ore deposits of the Great Basin: Reno, Geological Society of Nevada, p. 133-178.

Smith, J.T., and Booker, J.R., 1991, Rapid inversion of two-and three-dimensional magnetotelluric data: Journal, Geophysics Res., 96, 3905-3922.

Sternberg, B.K., Washburne, J., and Pellerin, L., 1988, Correction for the static shift in magnetotellurics using transient electromagnetic soundings: Geophysics, 53, 1459-1468.

Sutherland, D.B., 1967, AFMAG for electromagnetic mapping: Economic geology report #28, Mining and Groundwater Geophysics (Geol. Surv. of Canada), 228-237.

Torres-Verdin, C., 1991, Continuous profiling of magnetotelluric fields: Ph.D. thesis, University of California, Berkeley.

Torres-Verdin, C., and Morrison, H.F., 1991, Magnetotelluric analysis in the wavenumber domain, Abstract, 53rd Annual Mtg., EAEA, Florence, May 27-30, 398-399.

Torres-Verdin, C., and Bostick, F.X. Jr., 1992, Implications of the Born approximation for the magnetotelluric problem in three-dimensional environments: Geophysics, 57, 587-602.

Torres-Verdin, C., and Bostick F.X. Jr., 1992, Principles of spatial surface electric field filtering in magnetotellurics; Electromagnetic array profiling (EMAP): Geophysics, 57, 603-622.

Vozoff, K., 1991, The magnetotelluric method; in Nabighian, M.N., Ed., Electromagnetic methods in applied Geophysics, v2, Application, Chap. 8, S.E.G., Tulsa.

Wannamaker, P.E., Hohmann, G.W., and Ward, S.H., 1984, Magnetotelluric responses of three-dimensional bodies in layered earths: Geophysics, 49, 1517-1533.

Ward, S.H., O'Donnell, J., Rivera, R., Ware, G.H., and Fraser, D.C., 1966, AFMAG—applications and limitations: Geophysics, 31, 576-605.

Warren, R.K., and Srnka, L.J., 1992, Exploration in the basalt-covered areas of the Columbia River Basin, Washington, using electromagnetic array profiling (EMAP): Geophysics, 57, 986-993.

Yungul, S.H., 1966, Telluric sounding—A magnetotelluric method without magnetic measurements: Geophysics, 31, 185-191.

Zonge, K.L., and Hughes, L.J., 1991, Controlled source audio-frequency magnetotellurics; in Nabighian, M.N., Ed., Electromagnetic Methods in Applied Geophysics, v2, Application, Chap. 9, 713-809, S.E.G., Tulsa.